Photoelectrochemical Water Splitting Using Metal Oxides

INTERSHIP REPORT

Ravi Kishore [s1639641], Master's in Sustainable Energy Technology, University of Twente. Internship with Electrochemical Materials and Interfaces Group at:
DIFFER | DUTCH INSTITUTE FOR FUNDAMENTAL ENERGY RESEARCH | De Zaale 20, 5612 AJ Eindhoven, The Netherlands

ACKNOWLEDGEMENT

The present study was carried out at Dutch Institute For Fundamental Energy Research, Eindhoven under the guidance of Xueqing Zhang (Postdoc researcher) and Anja Bieberle (Dr. sc. Techn). The supercomputing facilities of Dutch national supercomputer Lisa/Surfsara were used to carry out the simulations.

CONTENTS

1. INTRODUCTION 4
2. ELECTROCHEMICAL MODEL 7
3. RESULTS AND DISCUSSION FOR WO_3 8
3.1. SURFACE ORIENTATION 9
3.2. DOPING 11
3.3. OXYGEN VACANCIES 14
4. RESULTS AND DISCUSSION FOR $BiVO_4$ 16
5. CONCLUSIONS 20
6. REFERENCES 21

LIST OF FIGURES

Figure 1-PEC cell in an acidic environment [2] 4
Figure 2-Requiremnts of a good semiconductor for water splitting [5] 5
Figure 3-(a) vacancy site (b) OH (c) O (d) OOH groups adsorbed on WO_3 surface, Tungsten atoms are represented by blue spheres, oxygen by red and Hydrogen by white 8
Figure 4-Free energy versus reaction step of the OER for pure (200), (020) and (002) surfaces of WO_3 10
Figure 5-Free energy step for different applied potentials 10
Figure 6 - W atom on the (200) surface replaced by a dopant atom 11
Figure 7- Free energy versus reaction step of the OER for pure and doped (200) WO_3 with reaction occurring on the W atom 12
Figure 8- Free energy versus reaction step of the OER for pure and doped (200) WO_3 with reaction occurring on the dopant atom 12
Figure 9-Free energy versus OER reaction step for pure and Mo doped WO3 on (002) surface 13
Figure 10-Free energy versus OER reaction step for pure and Mo doped WO3 on (020) surface 13
Figure 11- Oxygen vacancy structures for (200) surface. (a) Oxygen vacancy concentration 1.67/nm^2 (b) Oxygen vacancy concentration 0.41/nm^2 (c) Oxygen vacancy concentration 1.67/nm2, located two layers below the reaction site 14
Figure 12- Free energy versus reaction step of the OER for pure WO_3 and in the presence of oxygen vacancies 15
Figure 13-$BiVO_4$ reaction sites 16
Figure 14-Free energy versus reaction step for (040) surface of $BiVO_4$ 17
Figure 15-Free energy versus reaction step of OER on dopant atom introduced on Bi site, (040) surface $BiVO_4$ 17
Figure 16- Free energy versus reaction step of OER on dopant atom introduced on Bi site, (040) surface $BiVO_4$ 18
Figure 17-Free energy versus reaction step of the OER for (040) surface $BiVO_4$, when the dopant is introduced on V site while the reaction occurs on a different V site 19

LIST OF TABLES

Table 1- Gibb's Free energy value of each step of the OER among different surface orientations of WO3 9
Table 2-Gibb's Free energy value of each step of the OER for (200) surface when doped with Cr and Mo in different configurations 11
Table 3-OER on (020) and (002) surfaces of WO_3 13
Table 4 – OER steps with oxygen vacancies in (200) surface 15
Table 5-Free energy and overpotential for different reaction sites of (040) surface BiVO4 16
Table 6-EFFECT OF DOPING WHILE REACTION OCCURS ON DOPANT SITE, ON THE OVERPOTENTIAL OF $BIVO_4$ (040) SURFACE 17
Table 7-EFFECT OF DOPING AT V SITE ON THE OVERPOTENTIAL OF $BIVO_4$ (040) SURFACE, WHILE REACTION OCCURS ON DIFFERENT V SITE 18

1. INTRODUCTION

Energy storage is one of the biggest challenges facing the growth of renewable energy, especially wind and solar energy. Storage in the form of solar fuels like hydrogen and methanol is a promising solution [1]. Hydrogen can be produced by photo electrolysis of water by two routes, the indirect route where electricity from a photovoltaic (PV) generator can be transferred to an electrolysis unit or the direct route where hydrogen can be generated at the surface of a suitable semiconductor immersed in an electrolyte. This route if established could prove more efficient, cost effective and suitable to decentralized fuel production. The direct PV route requires high operating current densities ~ 1 A/cm^2 as compared to 10 to 20 mA/cm^2 for the photoelectrochemical (PEC) approach [2]. Thus the electrolyzers require a voltage of up to 1.9 V and since the thermodynamic required potential for water splitting is 1.23 V, this restricts their efficiencies to below 65%. The required overpotential for PEC cell is much lesser to reach the lower current densities hence they could have a much higher efficiency. A PEC unit may also be cheaper than a PV + electrolyzer unit because it is a single integrated unit.

The electrodes in PEC water splitting cell are made of semiconductor materials. Semiconductor materials have a band gap between conduction and valence bands, hence provide a possibility to separate electron hole pairs to provide the potential difference required to drive the reaction. These generated electrons and holes are responsible for production of hydrogen at cathode and oxygen at anode respectively in a photoelectrochemical cell as shown in Figure 1.

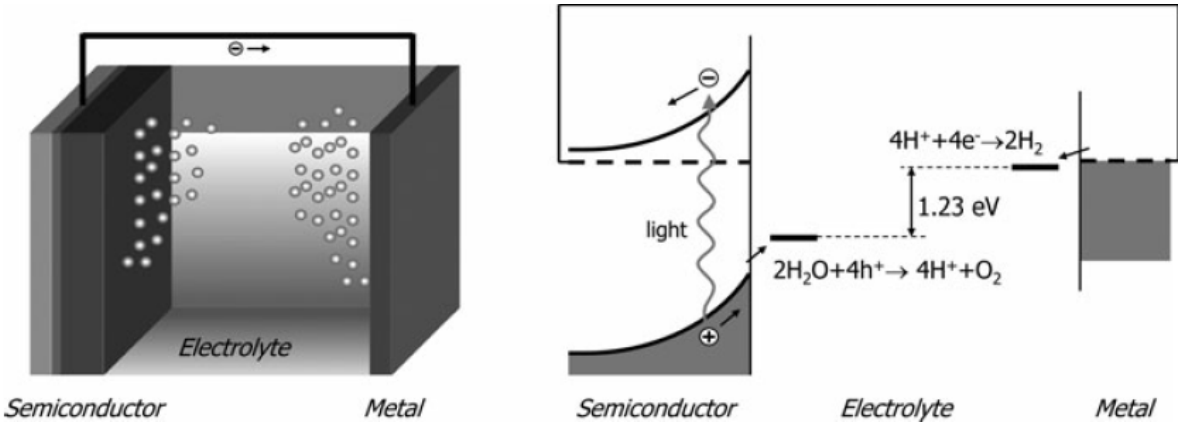

FIGURE 1-PEC CELL IN AN ACIDIC ENVIRONMENT [2]

The first demonstration of PEC water splitting was done by Fujishima et al. [3] on the surface of Titanium Oxide (TiO_2). Metal oxides are found to be stable in photochemical environments with a reasonable band gap. Hence they often attract interest for water splitting. Photochemical stability is one of the essential requirements of a semiconductor for carrying out PEC water splitting. This reason alone rules out Silicon based devices. A number of semiconductor metal oxides (example TiO_2, $NaTaO_3$) are capable of PEC water splitting, but they do so under UV wavelengths as shown in Figure 2. UV radiation forms a very small portion of solar spectrum hence these materials are not suitable for practical purposes. For visible light PEC water splitting a semiconductor must have a band gap less than 3.0 eV [4] . At the same time a minimum

band gap energy of 1.23 eV [2] is a must to drive the water splitting reaction. Also, the valence band and conduction band must be aligned separately to redox potentials of O_2 and H_2 respectively.

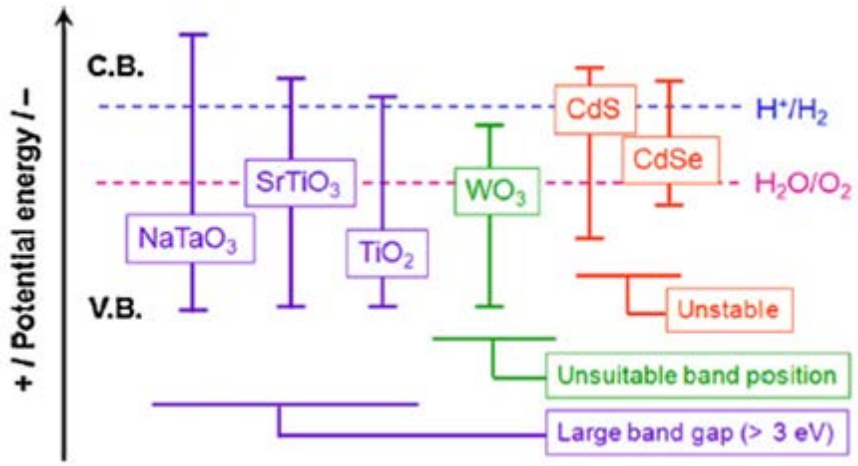

FIGURE 2-REQUIREMNTS OF A GOOD SEMICONDUCTOR FOR WATER SPLITTING [5]

Tungsten oxide (WO_3) is an interesting material for PEC water splitting because of its photochemical stability, a band gap (2.4 to 2.8 eV [6]) which favours visible light absorption and also has established high purity preparation methods. It is also known to be non-toxic and has n type semiconductor properties [7].

WO_3 has a small band gap and is found to be stable to photochemical processes, but shows low efficiency when used in its pure form. This is often attributed to fast recombination of electron-hole pairs, which could be resolved by doping it with other semiconductor materials. He, et al. [8], have found enhancement of photo catalytic activity in WO_3 when coupled with Sb_2O_3 through the photo-catalytic degradation of aqueous Rhb mixed with different WO_3/Sb_2O_3 samples. Ng, et al. [9] demonstrated band gap reduction from 2.74 eV to 2.60 eV and increase of photo activity of WO_3 when the anode was doped with 20% Gallium. Wang et al. [6] used doping with Mo and Cr ions, replacing W atoms in the lattice to demonstrate that though the band gap narrows down, but the conduction band also shifts down. Replacing O with S, however reduced the band gap and shifts the conduction band up, which is more favourable to the hydrogen evolution reaction. Doping with lower valence elements like Ti, Zr and Hf was also investigated. The band gap position and value was found to improve in these cases.

Similarly, monoclinic scheelite Bismuth Vanadate ($BiVO_4$) with a low band gap of 2.4 eV [4] is another material drawing a lot of research interest. Various researchers have attempted doping, coating with photo catalysts, forming hetro-junctions to improve the slow oxygen evolution kinetics for this material also.

Incorporation of 6 % Mo and 2% W during ballistic deposition of Bi, V, Mo and W at a deposition of angle of 55º has been found to increase the photocurrent densities up to 10 times [10]. An attempt will be made to confirm this by doping Mo and W into the lattice. Similarly, 0.5% PO4 doped BiVO4 has been found to increase the photocurrent density by about 30 times [11].

The present work focuses on density functional theory calculations of water oxidation reactions on WO_3 and $BiVO_4$ surfaces in various configurations of different surface orientations and doping and the analysis of calculated free energies and potential of rate determining steps. We will also perform the DFT calculations considering oxygen vacancies in the layers below the top surface as various studies report the improvement in performance of metal oxide photo anodes in the presence of oxygen vacancies [12]. It is found that these vacancies often promote electron hole separation which has a positive effect on water splitting efficiency.

2. ELECTROCHEMICAL MODEL

In a PEC splitting device, oxygen evolves at the semiconductor surface (anode) while electrons can be transported to a metal electrode (cathode) through a back contact where hydrogen evolution occurs. Water splitting reaction in an acidic environment can be understood as:

Cathode:

$$4H^+ + 4e^- \leftrightarrow 2H_2 \qquad E^0_{red} = 0.000\ \text{V SHE}$$

Anode:

$$2H_2O \leftrightarrow 4H^+ + O_2 + 4e^- \qquad E^0_{ox} = -1.229\ \text{V SHE}$$

For most metal oxides, oxygen evolution involves large over potential, hence there is a requirement to understand the mechanism involved for the oxygen evolution reaction (OER). We consider OER to proceed in following four single electron transfer steps:

$$2H_2O + O^* \rightarrow HOO^* + H_2O + H^+ + e^- \quad (A)$$

$$\rightarrow O^* + H_2O + 2H^+ + 2e^- \quad (B)$$

$$\rightarrow O^* + HO^* + 3H^+ + 3e^- \quad (C)$$

$$\rightarrow O_2 + 4H^+ + 4e^- \quad (D)$$

Density functional theory (DFT) calculations will be performed for each of the above reactions by considering that the reaction takes place on an individual atom on WO_3. The Gibb's free energy ΔG_U (U being the applied potential) for each step will be calculated and the maximum of these four values would be the rate limiting step. The calculations will be carried out using Vienna ab initio simulation package (VASP) developed by Fakultät für Physik of the Universität Wien. This tool carries out the calculation at applied potential U = 0, which may be corrected by $\Delta G_U = \Delta G_0 - eU$ where e is the number of total number of electrons generated till the given step. Thus, if a potential above rate limiting potential is applied all the steps in the reaction go downhill. In this manner, different configurations of a semiconductor surface can be compared. The configuration with minimum value of rate limiting potential could make the oxygen evolution most efficient.

3. Results and discussion For WO_3

We first obtain monoclinic WO_3 cell parameters from literature [13] and perform cell relaxation to get the most stable unit cell parameters with minimum free energy and pressure in the ion electron system. Then we obtain a bulk WO_3 structure with repeating cells and cleave it at the required surface. This structure is again submitted for surface relaxation to get a final test surface. We simulate four possible configurations of this surface viz. no specie attached to W site, i.e. vacancy site, HO- species attached to a W site, O- species attached to W site and HOO- species attached to a W site. These molecular geometries of (200) surface are shown in Figure 3:

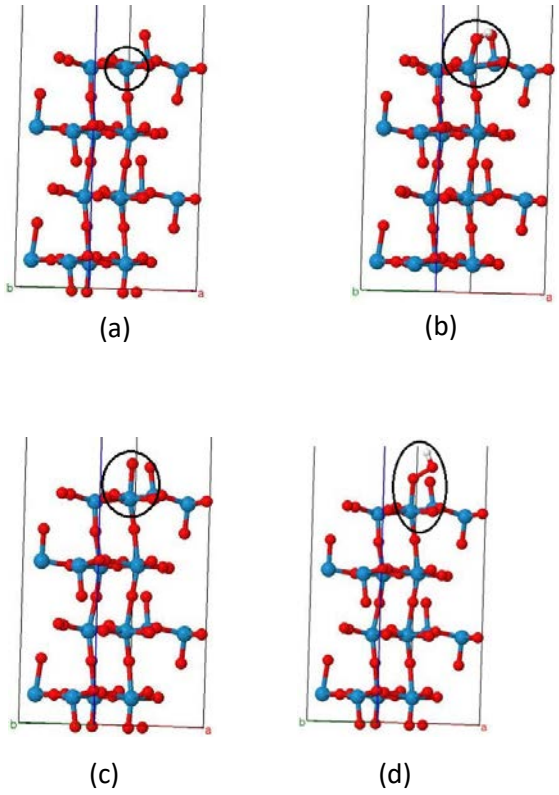

Figure 3-(a) vacancy site (b) OH (c) O (d) OOH groups adsorbed on WO_3 surface, Tungsten atoms are represented by blue spheres, oxygen by red and Hydrogen by white

We carry out the DFT calculations for each case till the results converge and record the final reaction energies. Gibb's free energies are calculated as:

$$\Delta G_0 = \Delta E + \Delta ZPE - T\Delta S$$

Where,

$\Delta G_0 = \Delta G(\text{Electrode potential}, U = 0, pH = 0, p = 1\text{bar}, T = 298\ K)$

$E =$ Reaction energy calculated from DFT

$ZPE =$ zero point energy from DFT calculation of vibrational frequencies

$S =$ Entropy from standard tables

The temperature dependence of enthalpy is neglected in the calculations. The interaction with neighbouring water molecules is neglected. The value of ΔG for the reaction $2H_2O \rightarrow O_2 + 2H_2$ is experimentally found to be 4.92 eV, hence the DFT calculations for formation of O_2 molecules may be avoided. The free energies of the reaction are finally calculated as [14]:

$$\Delta G_1 = \Delta E_{OH} - \Delta E_{vacancy} + 14.28 - 0.5 * 6.8 + 0.4$$
$$\Delta G_2 = \Delta E_O - \Delta E_{OH} - 0.5 * 6.8 - 0.37$$
$$\Delta G_3 = \Delta E_{OOH} - \Delta E_O + 14.28 - 0.5 * 6.8 + 0.39$$
$$\Delta G_4 = 4.92 - (\Delta G_1 + \Delta G_2 + \Delta G_3)$$

The overpotential may be defined and calculated as:

$$\eta = \max(\Delta G_1, \Delta G_2, \Delta G_3, \Delta G_4) - 1.23$$

3.1. SURFACE ORIENTATION

To study OER on WO_3 surface we will choose the (200), (020), and (002) surface orientations as these surfaces have been experimentally shown to have high photocurrent efficiency [15]. We performed the free energy calculations for each step of the OER on these surfaces with the following results:

Case #		ΔG_1 (eV)	ΔG_2 (eV)	ΔG_3 (eV)	ΔG_4 (eV)	η (eV)
i	WO_3 200 surface	1.52	2.02	1.39	-0.01	0.79
ii	WO_3 002 surface	2.36	2.23	0.33	0.00	1.13
iii	WO_3 020 surface	2.39	2.26	0.40	-0.14	1.16

TABLE 1- GIBB'S FREE ENERGY VALUE OF EACH STEP OF THE OER AMONG DIFFERENT SURFACE ORIENTATIONS OF WO3

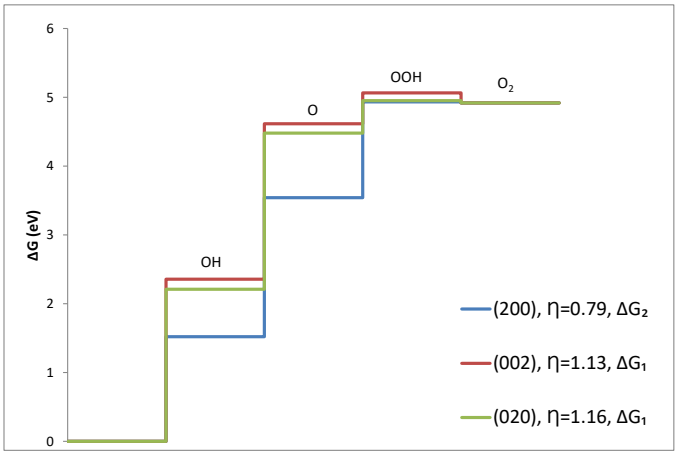

FIGURE 4-FREE ENERGY VERSUS REACTION STEP OF THE OER FOR PURE (200), (020) AND (002) SURFACES OF WO_3

Figure 4 compares the free energy versus reaction step for (200), (020) and (002) surfaces. It may be observed that (200) surface is the most favorable surface for OER as it offers the minimum over-potential. Also for both (020) and (002) surfaces, the rate limiting step is the 1st step i.e. adsorption of OH on to the surface, while for (200) surface it is the 2nd step i.e. the deprotonation step.

It may also be noted that for the (200) surface, the reaction steps remain uphill at the equilibrium potential of 1.23 V also, but if a bias voltage of $1.23 + \eta = 2.02V$ is applied, all reaction steps will become downhill. The same can be seen in Figure 5:

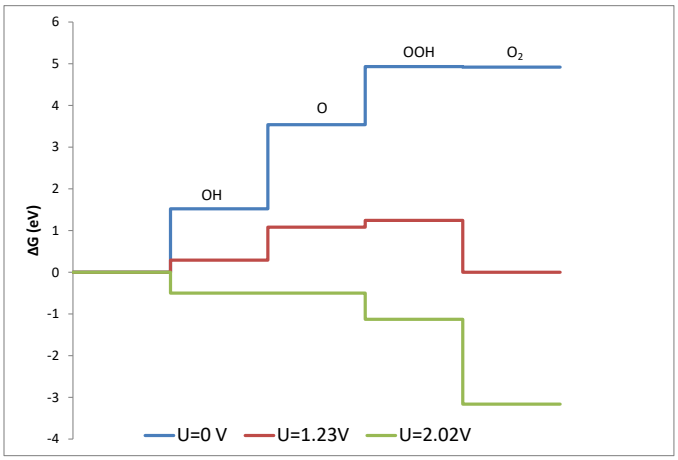

FIGURE 5-FREE ENERGY STEP FOR DIFFERENT APPLIED POTENTIALS

3.2. DOPING

We carry out Cr and Mo doping on (200) surface. We do this by substituting a W atom by the dopant atom in the geometry as shown in Figure 6:

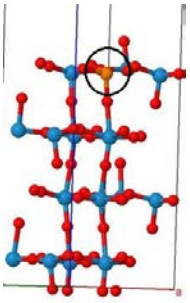

FIGURE 6 - W ATOM ON THE (200) SURFACE REPLACED BY A DOPANT ATOM

The dopant was introduced in two possible configurations, one where the reaction occurs on a W site and another when the reaction occurs on the dopant site. The results of these calculations are summarized in Table 2:

Case #		ΔG_1 (eV)	ΔG_2 (eV)	ΔG_3 (eV)	ΔG_4 (eV)	η (eV)
iv	Cr doping with reaction on W atom	1.31	2.25	1.05	0.30	1.02
v	Mo doping with reaction on W atom	1.43	2.15	1.38	-0.03	0.92
vi	Cr doping with reaction on Cr atom	2.14	1.77	1.00	0.01	0.91
vii	Mo doping with reaction on Mo atom	1.64	1.84	1.58	-0.14	0.61

TABLE 2-GIBB'S FREE ENERGY VALUE OF EACH STEP OF THE OER FOR (200) SURFACE WHEN DOPED WITH CR AND MO IN DIFFERENT CONFIGURATIONS

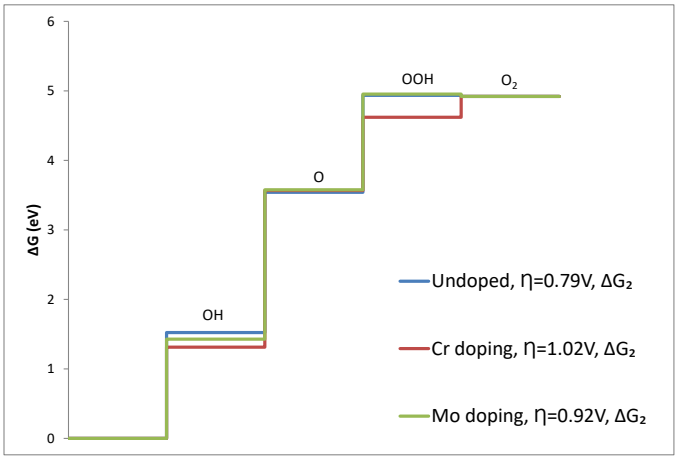

FIGURE 7- FREE ENERGY VERSUS REACTION STEP OF THE OER FOR PURE AND DOPED (200) WO_3 WITH REACTION OCCURRING ON THE W ATOM

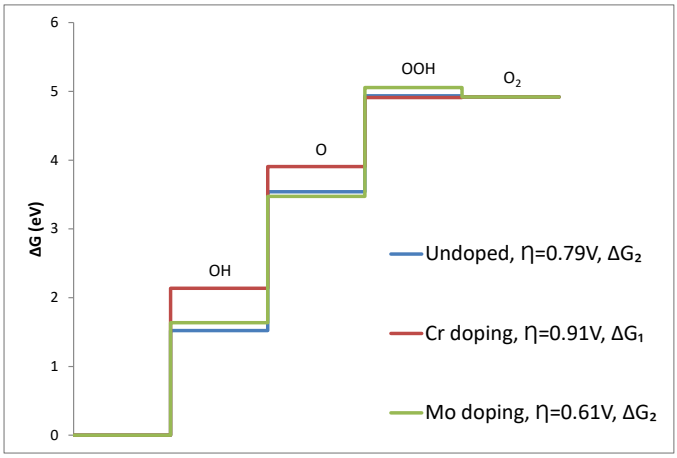

Figure 8- Free energy versus reaction step of the OER for pure and doped (200) WO_3 with reaction occurring on the dopant atom

A comparison of cases i, iv and v is illustrated in Figure 7. For all the three cases the formation of O from OH group is the rate limiting step. It may be observed that the rate limiting potentials do not improve by doping with either Cr or Mo when the reaction is occurring on the W site. Figure 8 compares cases i, vi and vii. In this case i.e. when reaction is occurring on dopant atom, for Cr doping, the rate limiting step is the adsorption of OH group on the Cr atom while for Mo doping it remains as the second step i.e. deprotonation. It may be observed Cr doping does not reduce the rate limiting potential however Mo doping reduces it. Thus, it may be concluded that reaction is likely to occur on Mo atom in case of doping and it will make the photoanode more efficient.

Further, we introduce Mo doping on (002) and (020) surfaces as well (cases viii to ix), and the results of the same are summarized in Table 3:

Case #		ΔG_1 (eV)	ΔG_2 (eV)	ΔG_3 (eV)	ΔG_4 (eV)	η (eV)
viii	WO_3 002 surface with Mo doping and reaction on Mo atom	2.62	2.02	0.45	-0.17	1.39
ix	WO_3 020 surface with Mo doping and reaction on Mo atom	2.52	1.98	0.64	-0.22	1.29

TABLE 3-OER ON (020) AND (002) SURFACES OF WO_3

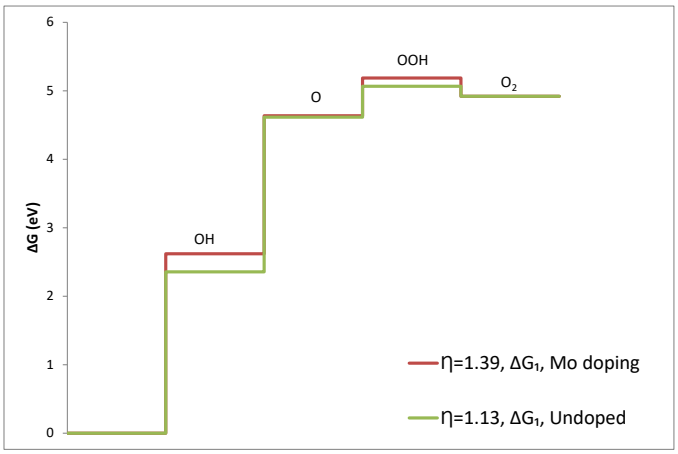

FIGURE 9-FREE ENERGY VERSUS OER REACTION STEP FOR PURE AND MO DOPED WO3 ON (002) SURFACE

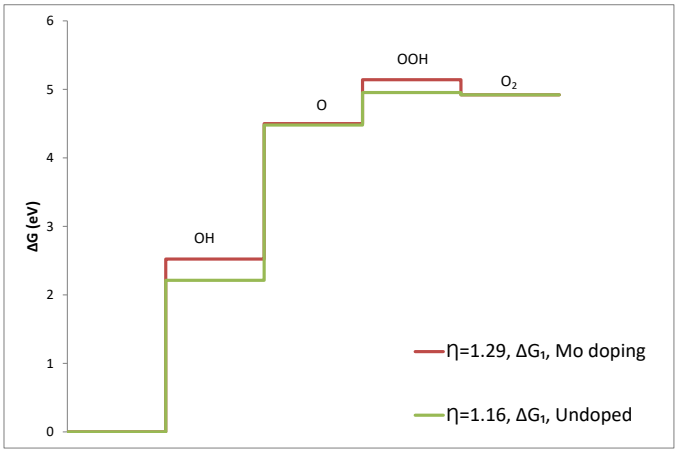

FIGURE 10-FREE ENERGY VERSUS OER REACTION STEP FOR PURE AND MO DOPED WO3 ON (020) SURFACE

From Figure 9 and Figure 10 it can be inferred that Mo doping for (002) and (020) surface increases the rate limiting potential. Hence it may be concluded that the reaction will proceed on the (200) surface in case of Mo doping as well, and will preferably occur on the Mo site.

3.3. OXYGEN VACANCIES

We also wish to analyze the effect of presence of oxygen vacancies in the WO_3 surface on the rate limiting step. As shown in Figure 11 (a), we first remove an oxygen directly below the reaction site, hence a concentration of 1.67/nm^2. Further we reduce this concentration to 0.41/nm^2 by increasing the surface area 4 times as shown in Figure 11 (b). In another possible configuration we keep the vacancy concentration 0.41/nm^2 but remove the oxygen atom 2 layers below and from a site which is not directly above the reaction site as shown in Figure 11 (c).

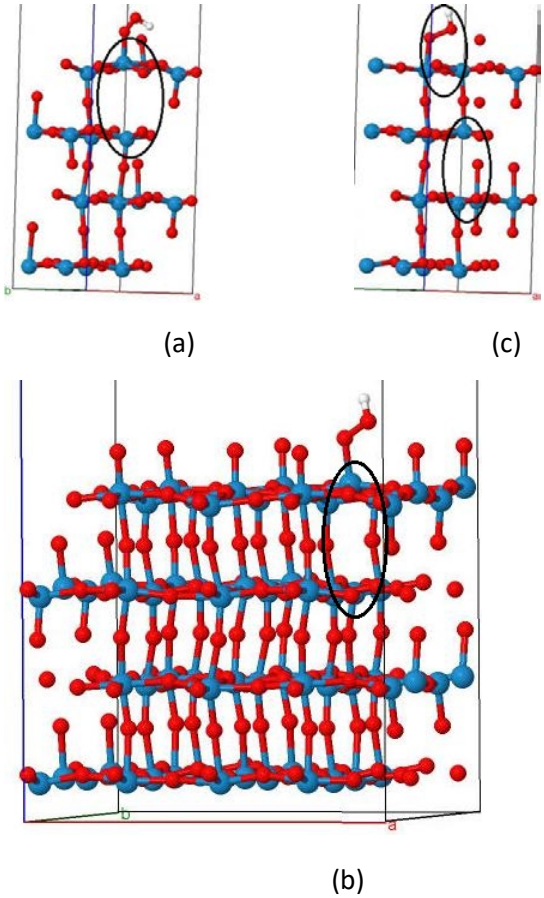

FIGURE 11- OXYGEN VACANCY STRUCTURES FOR (200) SURFACE. (A) OXYGEN VACANCY CONCENTRATION 1.67/NM^2 (B) OXYGEN VACANCY CONCENTRATION 0.41/NM^2 (C) OXYGEN VACANCY CONCENTRATION 1.67/NM2, LOCATED TWO LAYERS BELOW THE REACTION SITE

The results of the above simulations are shown in Table 4. Figure 12 demonstrates the effect of oxygen vacancies on the over-potential. For configuration shown in Figure 11 (a), two of the reaction steps the potential is negative which would mean the energy released in rearrangement of the lattice is more than the energy required for the reaction. Thus it may be concluded that for (200) surface of WO_3, oxygen vacancies lead to unstable restructuring of the lattice. For configuration, shown in Figure 11 (b) the concentration of oxygen vacancies was decreased to 1/4 by increasing the system size and keeping the number of oxygen vacancies the same and the overpotential was found to be still higher than the vacancy free surface. For configuration shown in Figure 11 (c), i.e. a geometry with oxygen vacancy two layers below in the original system size and with the reaction occurring on a tungsten atom which was not directly above, the free energy of the rate limiting step decreased and became even lesser than the vacancy free (200) surface. Zhang, et al. [16] found an optimum vacancy concentration to enhance the OER activity for hematite (110) surface. The reaction happens on the Fe atom above the vacancy. However, our simulations demonstrate that this is not applicable to WO_3. The vacancy increases the overpotential for two concentrations studied. The only way we found to improve the overpotential is that the OER occurs at a different site rather than the W site above the vacancy.

Case #		ΔG_1 (eV)	ΔG_2 (eV)	ΔG_3 (eV)	ΔG_4 (eV)	η (eV)
x	Configuration (a) Oxygen vacancy below the top layer, vacancy concentration 1.67/nm2	-1.18	-0.06	3.79	2.38	2.56
xi	Configuration (b) Oxygen vacancy below the top layer, vacancy concentration 0.41/nm^2	-1.74	0.90	2.73	3.04	1.81
xii	Configuration (c) Oxygen vacancy 2 layers below, but reaction on a W atom which is not directy above the vacancy with concentration 1.67/nm^2	0.73	1.44	1.86	0.89	0.63

TABLE 4 – OER STEPS WITH OXYGEN VACANCIES IN (200) SURFACE

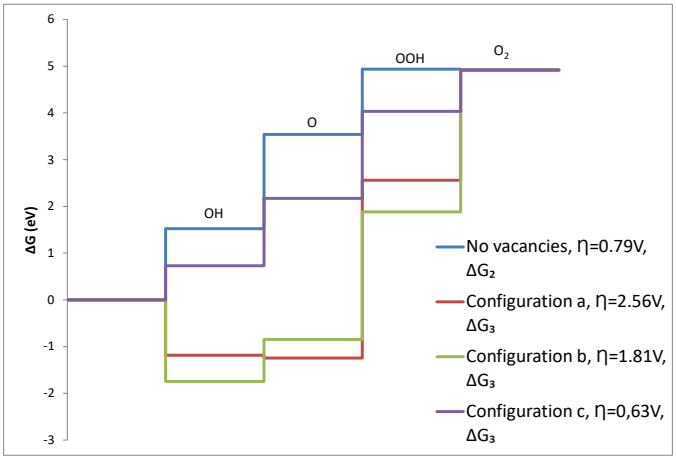

FIGURE 12- FREE ENERGY VERSUS REACTION STEP OF THE OER FOR PURE WO_3 AND IN THE PRESENCE OF OXYGEN VACANCIES

4. Results and discussion For $BiVO_4$

(040) surface of Monoclinic form of $BiVO_4$ is found to be more photo-catalytically active [5] and we shall use this surface for our simulation. There are three possible sites for the reaction i) Bi atom ii) V atom iii) Bridging oxygen atom as shown in Figure 13. We will use the same reaction mechanism as the one used for WO_3 and shall conduct similar DFT calculations with reactions occurring on the aforementioned reaction sites.

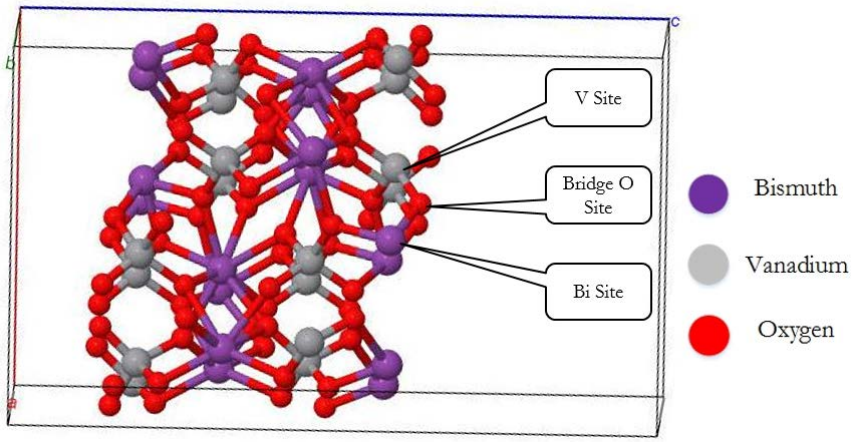

Figure 13-$BiVO_4$ reaction sites

The results of the simulation on each of the reaction site is tabulated in Table 5:

Case #	Configuration	ΔG_1 (eV)	ΔG_2 (eV)	ΔG_3 (eV)	ΔG_4 (eV)	η (eV)
i	Reaction on V site	1.48	1.96	1.47	0.01	0.73
ii	Reaction on Bridge site	1.96	1.49	1.74	-0.27	0.73
iii	Reaction on Bi site	2.17	1.72	1.41	-0.38	0.94

Table 5-Free energy and overpotential for different reaction sites of (040) surface $BiVO_4$

As can be seen from Figure 14, the V site and the bridge sites are the most active sites of this surface due to their lower overpotentials. Thus the reaction is more likely to proceed on these sites than the Bi site. It may also be noticed that the deprotonation step is the rate determining step for V site while for the other two sites it is the –OH adsorption step.

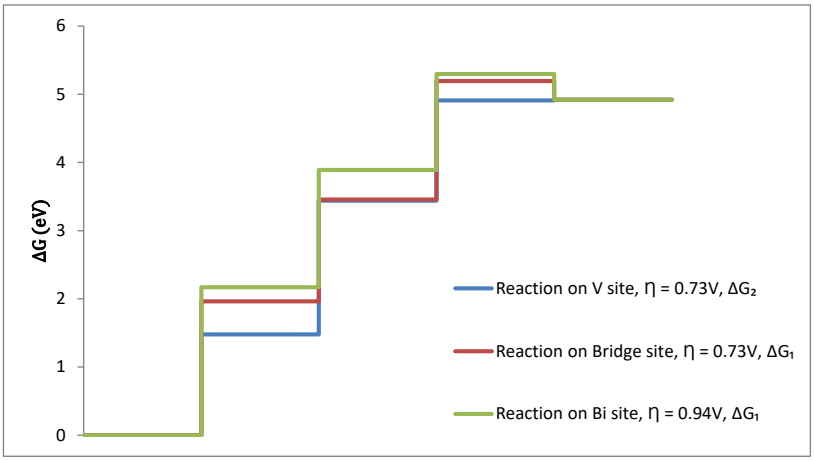

FIGURE 14-FREE ENERGY VERSUS REACTION STEP FOR (040) SURFACE OF $BiVO_4$

As previously mentioned, we also try the effect of doping with Mo and W in the surface. We introduce these dopants on V and Bi sites one by one. We also wish to check the effect of phosphate doping, hence we replace V site with P also and simulate the structures. The results of the simulations are summarized in Table 6 below:

Case #	Configuration	ΔG_1 (eV)	ΔG_2 (eV)	ΔG_3 (eV)	ΔG_4 (eV)	η (eV)
iv	W doping on Bi site	-0.27	-0.64	0.48	5.35	4.12
v	Mo doping on Bi site	-0.35	1.49	2.64	1.14	1.41
vi	W doping on V site	-0.54	1.85	1.43	2.18	0.95
vii	Mo doping on V site	-0.29	1.69	1.48	2.04	0.81
viii	P doing on V site	0.83	2.68	1.11	0.30	1.45

TABLE 6-EFFECT OF DOPING WHILE REACTION OCCURS ON DOPANT SITE, ON THE OVERPOTENTIAL OF $BiVO_4$ (040) SURFACE

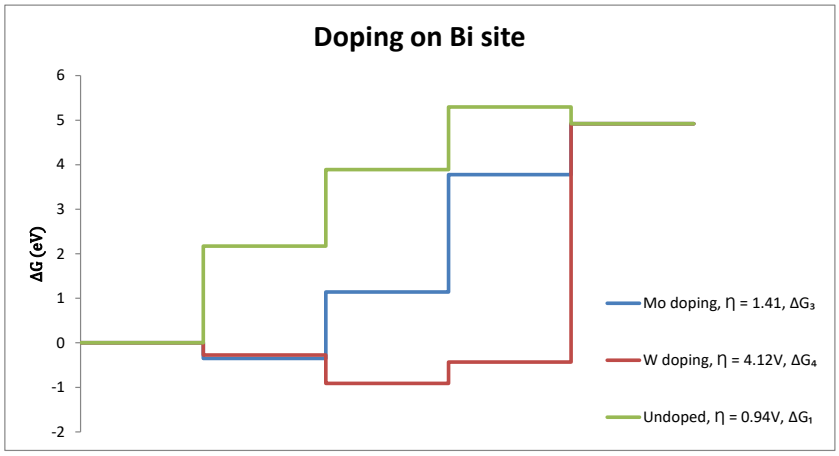

FIGURE 15-FREE ENERGY VERSUS REACTION STEP OF OER ON DOPANT ATOM INTRODUCED ON BI SITE, (040) SURFACE $BiVO_4$

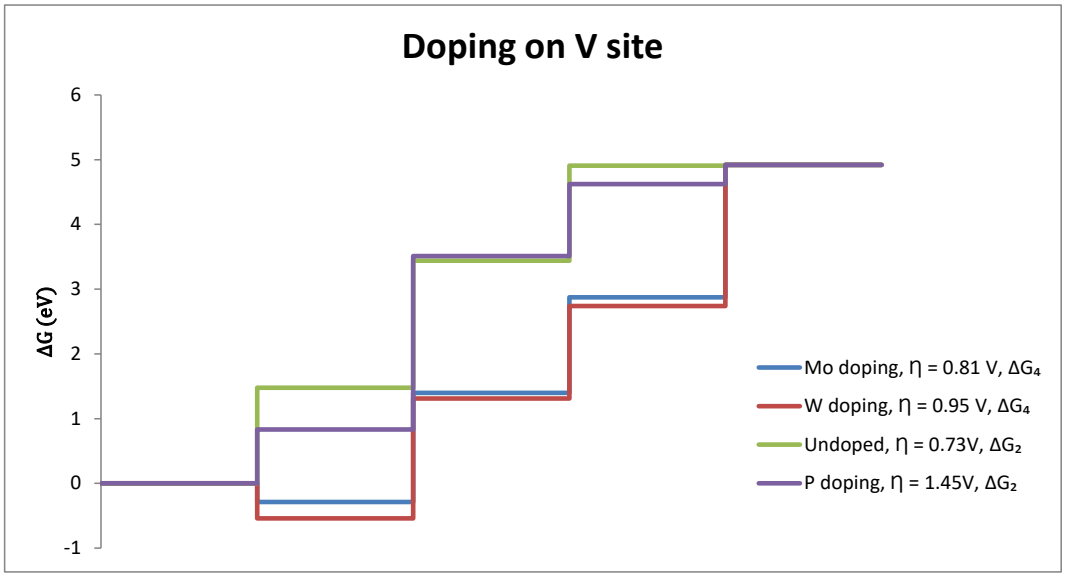

FIGURE 16- FREE ENERGY VERSUS REACTION STEP OF OER ON DOPANT ATOM INTRODUCED ON BI SITE, (040) SURFACE $BiVO_4$

From Figure 15 and Figure 16, it may be concluded that doping by Mo, W and P when the reaction occurs on the dopant site is not effective in reducing the overpotential for (040) surface of $BiVO_4$ irrespective of whether the dopant is introduced on Bi site or V site.

Thus we also try another configuration where dopant is introduced on the V site (already established as the most active), but the reaction is made to occur not on the dopant site but on a different V site. The results of these simulations are summarized in Table 7:

Case #	Configuration	ΔG_1 (eV)	ΔG_2 (eV)	ΔG_3 (eV)	ΔG_4 (eV)	η (eV)
ix	W doping on V site, reaction on different V site	-1.10	2.31	1.15	2.56	1.33
x	Mo doping on V site, reaction on a different V site	-1.12	2.30	1.14	2.60	1.37
xi	P doing on V site, reaction on a different V site	1.49	1.94	1.48	0.00	0.71

TABLE 7-EFFECT OF DOPING AT V SITE ON THE OVERPOTENTIAL OF $BiVO_4$ (040) SURFACE, WHILE REACTION OCCURS ON DIFFERENT V SITE

In this configuration, P doping improves the performance of the material while Mo and W doping again do not prove effective. It can also be concluded that on P doping the reaction is likely to occur on a V site instead of the P site.

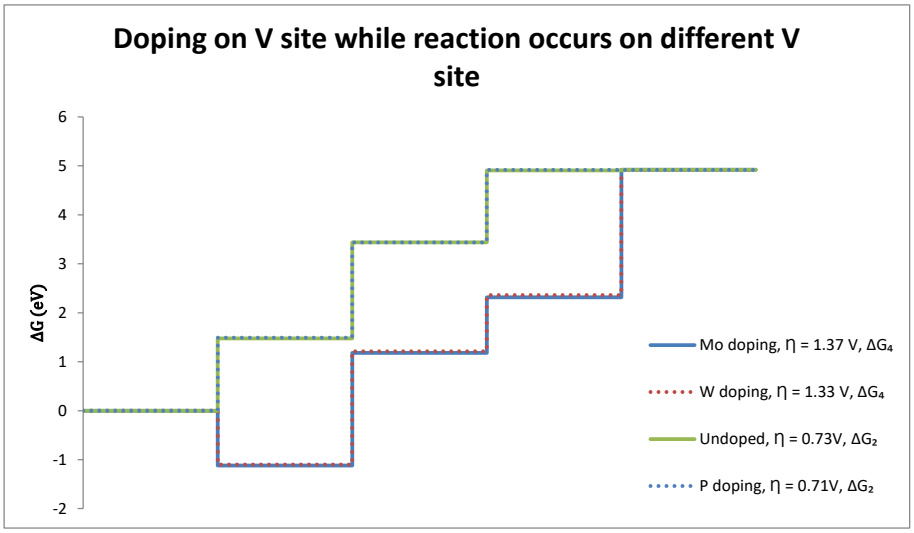

FIGURE 17-FREE ENERGY VERSUS REACTION STEP OF THE OER FOR (040) SURFACE $BiVO_4$, WHEN THE DOPANT IS INTRODUCED ON V SITE WHILE THE REACTION OCCURS ON A DIFFERENT V SITE

5. CONCLUSIONS

In the present work, it has been shown how DFT may be used to identify the most photo-chemically active surface of a metal oxide. A method to test the effect of doping in the crystal has also been developed which could help the experimentalists working in this field. This helps to understand the OER better, as we identify the active sites on the surface of the metal oxide where reaction is most likely to occur. We also know the rate limiting step in the OER mechanism, which could help in the designing of good co-catalysts.

For WO_3, we conclude that the (200) surface is the most photo active surface of WO_3 and further Mo doping is effective in reducing the rate limiting over-potential for this surface. The dopant was found to be more effective when the reaction occurs on the dopant site than when the reaction occurs on the W atom. Mo doping does not help the (020) and (002) surfaces to decrease the rate limiting over-potential. Hence, the reaction will most likely occur on (200) surface even in case of doping. It can also be concluded that presence of oxygen vacancies may help to decrease or increase the overpotential of the rate limiting step depending upon its position in the geometry.

For $BiVO_4$, the V site was identified as the most active site for water splitting. Introducing dopants on V site was found to be more effective than Bi site. Also Phosphorous was identified as a good dopant for the same. It was also concluded that the reaction was likely to occur on another V site in case of P doping.

6. REFERENCES

[1] S. B. et al., "Towards Artificial Leaves for Solar Hydrogen and Fuels," *Chemsuschem,* vol. 5, pp. 500-521, 2012.

[2] K. R. et al., "Benchmark for Photoelectrochemical Water Splitting," in *Photoelectrochemical Hydrogen Production*, Springer Science + Business Media, 2012, p. 9.

[3] A. F. et al., "Electrochemical Photolysis of Water at a Semiconductor Electrode," *Nature,* vol. 238, pp. 37-38, 1972.

[4] C. S. et al., "BiVO4 as photo catalyst for solar fuels production through water splitting : A short review," *Applied Catalysis A: General,* vol. 504, pp. 158-170, 2015.

[5] C. M. S. et al., "BiVO4as photocatalyst for solar fuels production through watersplitting: A short review," *Applied Catalysis A: General,* vol. 504, pp. 158-170, 2015.

[6] F. W. et al., "Doping of WO3 for Photo-catalytic Water Splitting: Hints from Density Functional Theory," *The Journal of Physical Chemistry C,* vol. 116, pp. 8901-8909, 2012.

[7] S. J. Y. et al., "Tungsten oxide bilayer electrodes for photoelectrochemical cells," *Journal of Power Sources,* vol. 195, no. 16, p. 5422–5425, 2010.

[8] H. G.-H. et al., "Preparation of novel Sb2O3/WO3 photo-catalysts and their activities under visible light irradiation," *Materials Research Bulletin,* vol. 48, pp. 2244-2249, 2013.

[9] K. H. N. et al., "Gallium-doped tungsten trioxide thin film photo-electrodes for photo-electrochemical water splitting," *International Journal of Hydrogen Energy,* vol. 38, pp. 1-7, 2013.

[10] S. B. et al., "Incorporation of Mo and W into nanostructured BiVO4 films for efficient photoelectrochemical water oxidation," *Phys. Chem. Chem. Phys.,* vol. 14, pp. 7065-7075, 2012.

[11] W. J. et al., "Phosphate Doping into Monoclinic BiVO4 for Enhanced Photoelectrochemical Water Oxidation Activity," *Angewandte Chemie,* vol. 51, pp. 3147-3151, 2012.

[12] C. Z. et al., "Plasma-Induced Oxygen Vacancies in Ultrathin Hematite Nanoflakes Promoting Photoelectrochemical Water Oxidation," *ACS Applied Materials and interfaces,* vol. 7, pp. 22355-22363, 2015.

[13] T. V. et al., "The High-Temperature Phases of WO3," *Journal of Solid State Chemistry,* vol. 144, pp. 209-215, 1999.

[14] Á. V. et al., "First principles study of the photo-oxidation of water on tungsten trioxide (WO3)," *The Journal of Chemical Physics,* vol. 130, pp. 114701-9, 2009.

[15] C. S. et al., "Photo electrochemical Properties of Nanostructured Tungsten Trioxide Films," *Journal of Physical Chemistry B,* vol. 105, pp. 936-940, 2001.

[16] X. Z. et al., “Oxygen Evolution at Hematite Surfaces: The Impact of Structure and Oxygen Vacancies on Lowering the Overpotential,” *The Journal of Physical Chemistry C,* vol. 120, pp. 18201-18208, 2016.